Trakya University Journal of Natural Sciences, 27(1), xx–xx, 2026
DOI: 10.23902/trkjnat.2025715
www.tujns.org

Research Article

In silico characterization of *Plasmodium falciparum* FabI: Implications for the design of antimalarial drugs

Abdelaziz Brkhan[1], Hajar Almuree[1], Dima Joujeh[2]*

[1]*University of Aleppo, Faculty of Technical Engineering, Department of Biotechnology Engineering, Aleppo, Syria*
[2]*University of Aleppo, Faculty of Technical Engineering, Ph.D. in Biotechnology Engineering, Aleppo, Syria*

Cite this article as: Brkhan, A., Almuree, H., & Joujeh, D. (2025). *In silico* characterization of *Plasmodium falciparum* FabI: Implications for the design of antimalarial drugs. *Trakya University Journal of Natural Sciences, 27*(1), xx–xx.

Abstract

Background: The FabI enzyme, crucial for fatty acid synthesis, represents a promising target for antimalarial drug development, particularly in *Plasmodium falciparum*.

Aims: To comprehensively characterize the *P. falciparum* FabI enzyme by elucidating its evolutionary relationships, physicochemical properties, and detailed structural features using advanced *in silico* methodologies.

Methods: An extensive computational analysis was performed on 25 FabI protein sequences, encompassing those from *P. falciparum* as well as diverse protozoan and bacterial species.

Results: The predicted physicochemical properties indicated that *P. falciparum* FabI is compartively larger, more hydrophilic, and exhibits a higher isoelectric point than its bacterial homologs. Sequence alignment and phylogenetic reconstruction revealed a clear evolutionary divergence of *P. falciparum* FabI from bacterial orthologs, supporting its origin through an ancient horizontal gene transfer event and its localization to the apicoplast. Further sequence analysis identified two conserved motifs mapped to a central NAD(P) binding Rossmann-fold domain, which is essential for the enzyme's catalytic function. The predicted three-dimensional (3D) structure of *P. falciparum* FabI exhibited a characteristic α/β-fold architecture forming a dimeric complex. A persistent challenge was noted in the N-terminal region, predicted to be a flexible, cleavable signal/transit peptide, accounting for its lower structural confidence. PDBsum analysis delineated its structural organization, consisting of 19 α-helices and 9 β-strands, with a notable absence of disulfide bridges. Additionally, proteolytic digestion produced multiple cleavage patterns. CASTp 3.0 analysis revelaed a complex active site comprising several sub-pockets and key functional residues, along with buried cavities.

Özet

Dayanak: Yağ asidi sentezi için çok önemli olan FabI enzimi, özellikle *Plasmodium falciparum*'da sıtma ilacı geliştirme için umut verici bir hedef oluşturmaktadır.

Amaçlar: Çalışma, gelişmiş in silico metodolojileri kullanarak evrimsel ilişkilerini, fizikokimyasal özelliklerini ve ayrıntılı yapısal özelliklerini aydınlatarak *P. falciparum* abI enzimini kapsamlı bir şekilde karakterize etmeyi amaçlamıştır.

Yöntemler: *P. falciparum*'dan ve çeşitli protozoa ve bakteri türlerinden alınan 25 FabI protein dizisi üzerinde kapsamlı bir hesaplamalı analiz gerçekleştirilmiştir.

Bulgular: Tahmin edilen fizikokimyasal özellikler, *P. falciparum* FabI'nin bakteriyel homologlarına kıyasla daha büyük, daha hidrofilik ve daha yüksek izoelektrik noktaya sahip olduğunu göstermiştir. Sekans hizalama ve filogenetik rekonstrüksiyon, *P. falciparum* FabI'nin bakteriyel ortologlarından açık bir evrimsel farklılık gösterdiğini ortaya koymuş ve bunun eski bir yatay gen transferi olayı yoluyla kökenini ve apikoplastta lokalizasyonunu desteklemiştir. Daha ileri sekans analizi, enzimin katalitik fonksiyonu için gerekli olan merkezi NAD(P) bağlayıcı Rossmann-fold alanına eşlenen iki korunmuş motif tanımladı. *P. falciparum* FabI'nin tahmin edilen üç boyutlu (3D) yapısı, dimerik bir kompleks oluşturan karakteristik bir α/β-fold mimarisi sergiledi. N-terminal bölgesinde, esnek, bölünebilir bir sinyal/geçiş peptidi olduğu tahmin edilen ve yapısal güvenilirliğinin düşük olmasına neden olan kalıcı bir zorluk tespit edildi. PDBsum analizi, disülfür köprülerinin belirgin bir şekilde yokluğuyla, 19 α-heliks ve 9 β-iplikçikten oluşan yapısal organizasyonunu ortaya koydu. Ek olarak, proteolitik sindirim çoklu bölünme modelleri üretti. CASTp 3.0 analizi, gömülü boşluklarla birlikte birkaç alt cep ve önemli fonksiyonel kalıntılardan oluşan karmaşık bir aktif bölge ortaya çıkardı.

Edited by: *Özkan Danış*

***Corresponding Author:** Dima Joujeh, **E-mail:** dimajoujeh@gmail.com*

***ORCID iDs of the authors:** AB. 0009-0007-4042-9062; HA. 0009-0005-3177-7693; DJ. 0000-0001-8240-9886*

Received: 13 August 2025, **Accepted:** 7 October 2025, **Epub:** 12 November, 2025

Copyright© 2025 The Author(s). Published by Galenos Publishing House on behalf of Trakya University.
Licensed under a Creative Commons Attribution (CC BY) 4.0 International License.

OPEN ACCESS

Conclusion: These comprehensive structural and functional insights into the unique features of *P. falciparum* FabI provide a strong foundation for the rational design of novel antimalarial drugs.

Sonuç: *P. falciparum* FabI'nin benzersiz özelliklerine ilişkin bu kapsamlı yapısal ve fonksiyonel bilgiler, yeni sıtma ilaçlarının rasyonel tasarımı için güçlü bir temel sağlar.

Keywords: *Plasmodium falciparum*, FabI enzyme, phylogenetic analysis, conserved motifs, protein structure prediction

Introduction

Malaria, a febrile disease, is caused by *Plasmodium* parasites transmitted to humans through the bites of infected female *Anopheles* mosquitoes (A. Pandey et al., 2022). The growing resistance of malaria parasites to first-line therapies highlights the urgent need to develop new classes of antimalarial agents (Kane et al., 2022). Consequently, the systematic identification and detailed characterization of unique parasite biochemical pathways have become essential, as these pathways provide promising targets for both novel drug discovery and the optimization of existing or emerging therapeutic strategies (A. K. Pandey et al., 2019).

These intracellular parasites depend on lipids for their growth, proliferation, and developmental progression. They utilize a prokaryotic-like Type II fatty acid synthesis (FAS-II) system housed within the apicoplast, an organelle crucial for the parasite's blood-stage replication and overall pathogenicity (A. Pandey et al., 2022). Thus, the parasite's fatty acid biosynthesis (FAS-II) pathway has emerged as a compelling therapeutic target due to its essential role in parasite viability (Kane et al., 2022). The distinct organization of the FAS-II pathway, when compared to the mammalian FAS-I complex, highlights its unique potential as a selective drug target.

FabI, the principal enoyl-ACP reductase within the FAS II system, is among the most extensively studied enzyme of this pathway. It is widely conserved across mutile microorganisms, including *Staphylococcus aureus*, *Escherichia coli*, *Bacillus subtilis*, *Francisella tularensis*, *Burkholderia pseudomallei*, *Bacillus anthracis*, *Pseudomonas aeruginosa*, as well as the protozoan parasites *Toxoplasma gondii* (Hopf et al., 2022), and *Plasmodium falciparum* (Kane et al., 2022). Given its pivotal role across a braod spectrum of pathogens, an in-depth understnading of FabI's molecular and structural characteristics is of critical importance for guiding drug discovery efforts.

In recent years, *in silico* methodologies have become integral to modern drug discovery, offering powerful means to charaterize molecular targets and facilitate rational inhibitor design. These computational approaches allow precise delineation of a protein's molecular properties, encompassing sequence architecture, physicochemical behavior, and evolutionary lineage, while identifting key functional elements such as conserved motifs, catalytic residues, and signal peptides. Such insights can be obtained prior to experimental validation or large-scale screening.

This study aimed to comprehensively characterize the *P. falciparum* FabI enzyme by elucidating its evolutionary relationships, physicochemical features, and intricate structural organization using advanced *in silico* technoiques. The resulting findings establish a strong foundation for the rational design of selective FabI inhibitors, thereby contributing to the development of nest-generation antimalarial therapeutics.

Materials and Methods

Sequence Retrieval and Alignment

Twenty-five enoyl-ACP reductase (FabI) sequences, representing both bacterial and eukaryotic (protozoan) origins, were retrieved from the UniProt (https://www.uniprot.org) (The UniProt Consortium, 2024). Sequence selection emphasized phylogenetic diversity and clinical relevance to human pathogenicity. Accession numbers for all sequences are listed in Supplementary Table 1. Multiple sequence alignments were generated using the Clustal Omega algorithm (https://www.ebi.ac.uk/Tools/msa/clustalo/) (Madeira et al., 2024). The resulting alignments were visually examined and verified through manual inspection with the UniProt Alignment Viewer to ensure accurate alignment of conserved residues and the logical placement of gap regions.

Determination of Physicochemical Parameters

The physicochemical characteristics of FabI enzymes were computed from their amino acid sequences using the ExPASy ProtParam tool (http://web.expasy.org/protparam) (Gasteiger et al., 2005). The calculated parameters included molecular weight, isoelectric point (pI), extinction coefficient (EC), instability index (II), aliphatic index (AI), and grand average of hydropathicity (GRAVY).

Phylogenetic Tree Construction

A phylogenetic tree was constructed using the aligned amino acid sequences with the Simple Phylogeny tool available through EMBL-EBI (https://www.ebi.ac.uk/jdispatcher/phylogeny/simple_phylogeny) (Madeira et al., 2024). Evolutionary relationships among the taxa were inferred using the Neighbor-Joining algorithm, which operates on a pairwise distance matrix derived from the multiple sequence alignment.

Primary Structure Analysis

Primary structure analysis was conducted using the ExPASy ProtParam tool, specifically to determine the amino acid composition. Conserved protein motifs were identified with the MEME suite (http://meme.sdsc.edu/meme/meme.html) (Bailey & Elkan, 1994). Protein domains were examined using InterProScan (http://www.ebi.ac.uk/interpro/search/sequence/) (Blum et al., 2024).

Secondary Structure Analysis

The secondary structural content of the FabI sequences, including alpha helices, beta turns, extended strands, and random coils, was predicted using the SOPMA method available through the Network Protein Sequence Analysis (NPS@) server (https://npsa-prabi.ibcp.fr/cgibin/npsa_automat.pl?page=npsa_sopma.html) (Geourjon & Deléage, 1995).

Tertiary structure prediction for *P. falciparum* FabI was generated using ColabFold, an optimized AlphaFold2 implementation created for accelerated protein structure prediction. ColabFold was assessed through the COSMIC platform (https://cosmic-cryoem.org/tools/colabfold/) (Mirdita et al., 2021), and the resulting three-dimensional (3D) structural model was subsequently visualized using PyMOL.

The predicted 3D structure was further interpreted through the PDBsum tool (https://www.ebi.ac.uk/thornton-srv/databases/cgibin/pdbsum/GetPage.pl?pdbcode=index.html), which provided a secondary motif map and topology diagram. Predicted disulfide bridge patterns were evaluated using the CYS-REC tool (http://softberry.com/berry.phtml), allowing the identification of probable disulfide bonding between available Cysteine (Cys) residues.

Tertiary Structure Validation

The *P. falciparum* FabI model underwent extensive validation using multiple computational approaches. QMEAN (https://swissmodel.expasy.org/qmean) was employed to assess both global and local model quality (Benkert et al., 2010; Studer et al., 2014, 2019). Additional validation was performed through the SAVES server (https://servicesn.mbi.ucla.edu/SAVES) (Colovos & Yeates, 1993; Laskowski et al., 1996), which produced a Ramachandran plot using PROCHECK, and evaluated structural error rates using ERRAT. The Ramachandran plot served as the primary stereochemical quality indicator, while ERRAT confirmed crystallographic model accuracy. Predicted salt bridges were also analyzed using dedicated protein analysis tools.

Functional Analysis

Proteolytic cleavage sites, including those produced by chemical reagents, were predicted using PeptideCutter (http://web.expasy.org/peptide_cutter/) (Gasteiger et al., 2005). Signal peptide regions were prediction with SignalP 6.0 (https://services.healthtech.dtu.dk/services/SignalP-6.0/) (Teufel et al., 2022), which detects all five known signal peptide types (Sec/SPI, Sec/SPII, Tat/SPI, Tat/SPII, Sec/SPIII). The Computed Atlas of Surface Topography of proteins (CASTp 3.0) server (http://sts.bioe.uic.edu/) was used to identify active binding site pockets and to analyze the protein surface topography (Tian et al., 2018).

Results

Sequence Retrieval and Alignment

The protein sequences of FabI enzymes from a range of bacterial strains and protozoa were retrieved from UniProt, with FASTA format sequences selected and prioritized based on pathogens relevant to human health, as indicated in UniProt (Supplementary Table 1).

Homology searching followed by multiple sequence alignment of the 25 FabI enzyme sequences revealed several regions of high conservation. The alignment displayed two particularly well conserved motifs, AKAALES (326–332), and RVNAISAGPIRT (348–359) (Figure 1). In addition to these conserved stretches, a set of 16 amino acid positions demonstrated 100% conservation across all sequences examined. These residues included Glycine (Gly) 128, Aspartic acid (Asp) 206, Histidine (His) 252, Serine (Ser) 282, Ser 285, Tyrosine (Tyr) 309, Tyr319,

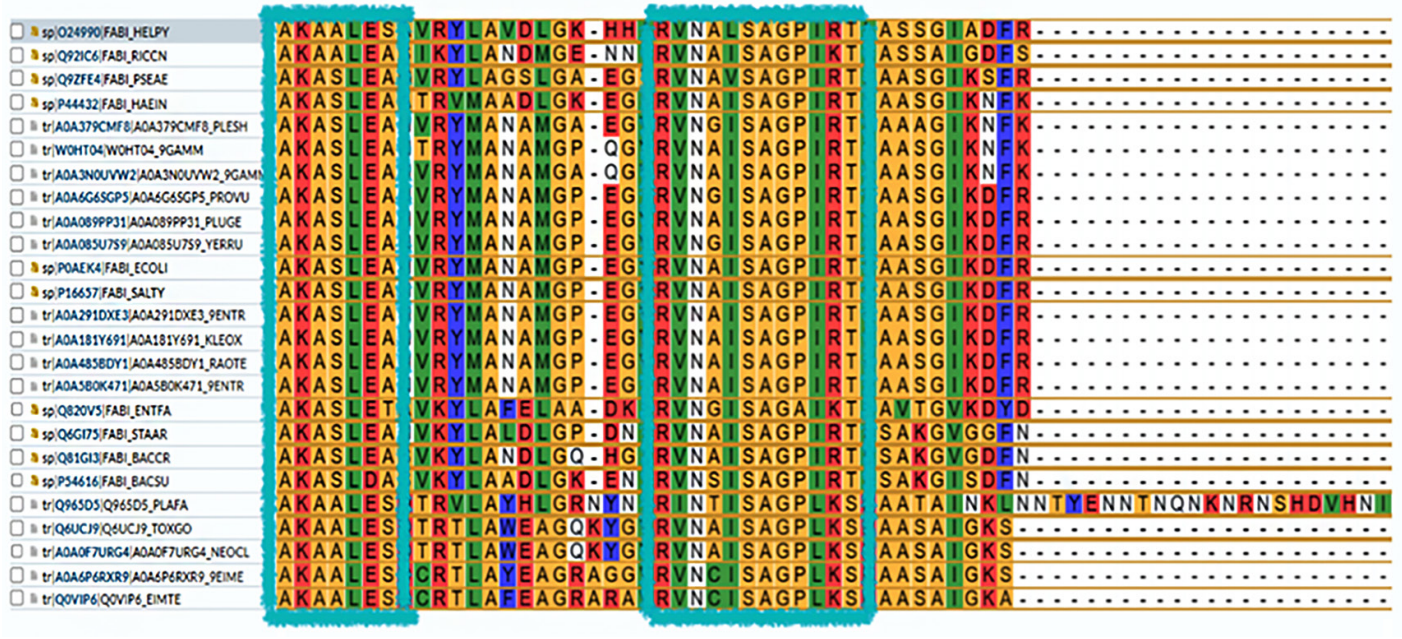

Figure 1. Close-up of multiple sequence alignment showing conserved motifs (cyan boxes).

Methionine 323, Alanine (Ala) 338, Gly434, Leucine (Leu) 440, Ser 442, Gly450, Valine 455, Asp456, and Gly458. Collectively, these fully conserved residues represented a braod spectrum of amino acid classes, including: nonpolar (Ala, Leu, Gly, Methionine, Valine), polar (Ser), aromatic (Tyr), acidic (Asp), and basic (His).

Phylogenetic Analysis of FabI Enzyme Sequences

The unrooted phylogenetic tree (Figure 2), constructed from FabI enzyme protein sequences, depicts the evolutionary relationships among the sampled bacterial and protozoan taxa. *Plasmodium* (evolutionary distance: 0.31445) is positioned within a distinct and well-supported clade of Apicomplexa parasites, clustering with *Neospora* (0.05476), *Toxoplasma* (0.06203), *Cyclospora* (0.10345), and *Eimeria* (0.11790). These taxa form a compact clade with short internal branch lengths, suggesting a recent common evolutionaty origin among these protozoan parasites. The entire *Plasmodium*-containing clade remains clearly separated from all bacterial taxa represented in the tree, indicating substantial evolutionary divergence.

Physicochemical Properties of FabI Enzymes

Analysis of physicochemical properties demonstrated both shared features and distinct differences across FabI enzymes from protozoa and bacteria (Table 1). FabI enzymes from protozoan parasites were generally longer (393–432 amino acids), and possessed higher molecular weights (approximately 40–49 kDa), whereas bacterial FabI proteins were typically shorter (250–275 amino acids) with lower molecular weights (26–30 kDa).

Isoelectric point (pI) values also displayed a clear taxonomic distinstion: protozoan FabI enzymes displayed higher pIs (6.01–9.11), with *P. falciparum* displaying the highest pI at 9.11, while most bacterial FabI enzymes had lower pI values (5.15–5.77). Notably, *Helicobacter pylori* (pI 7.1) and *Rickettsia conorii* (pI 7.71) were exceptions to this trend.

The AI indicated that a tendency toward greater alipahtic content among bacterial FabI proteins (85.92–105.72) compared to protozoan FabI (77.92–91.46), with *Enterococcus faecalis* demonstrating the highest value. GRAVY values similarly highlighted these differences: protozoan FabI enzymes displayed more hydrophilic properties (negative GRAVY values from 0.046 to −0.683), with *P. falciparum* being the most hydrophilic, whereas bacterial FabI enzymes were slightly hydrophobic (positive GRAVY values from 0.012 to 0.191). Instability indices for most FabI proteins were below 40, indicating overall structural stability, although *P. falciparum* showed a slightly higher instability value (45.92).

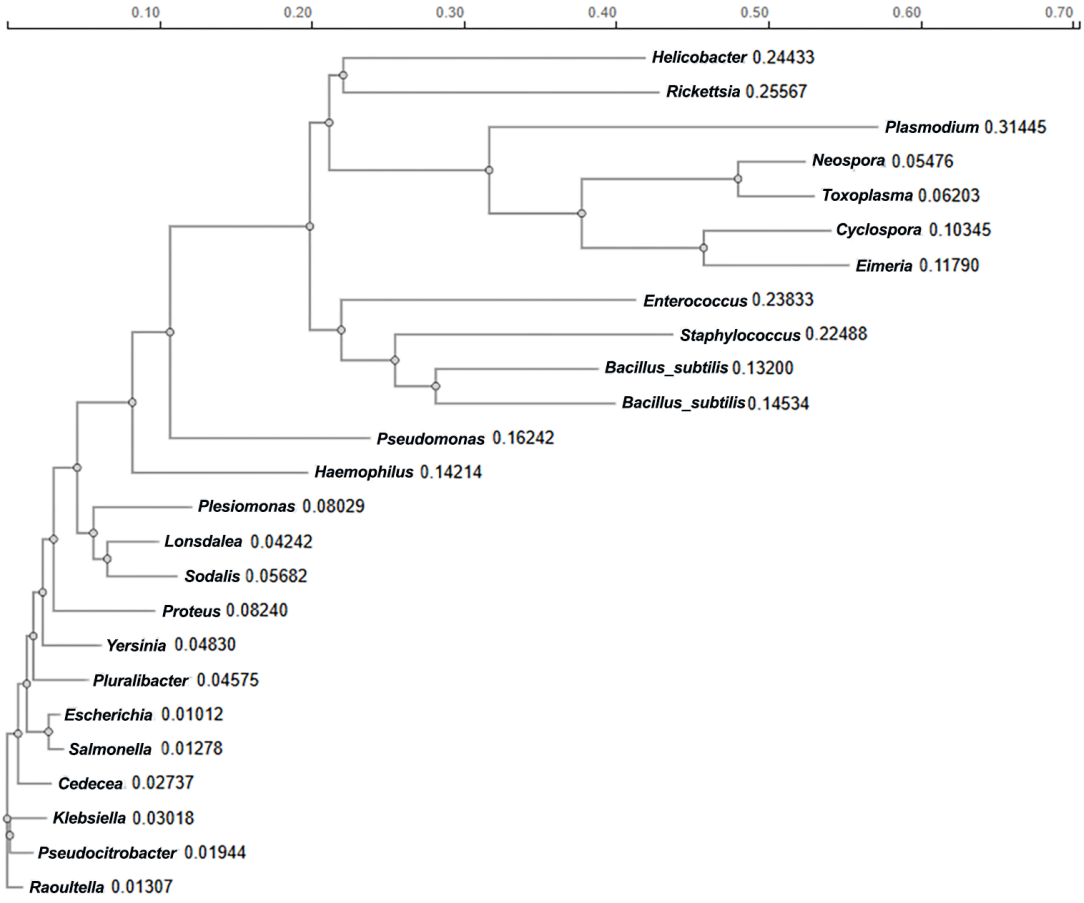

Figure 2. Unrooted phylogenetic tree of FabI enzyme sequences.

Protozoan FabI enzymes also contained larger numbers of both acidic (R- values from 35–47) and basic (R+ values from 35–57) residues compared to their bacterial FabI sequences, which typically contained fewer acidic (25–33) and basic (21–28) residues. In accordance with this trend, ECs were higher for protozoan enzymes (27390–48360) than for bacterial ones (13075–21680), aside from *H. pylori* and *R. conorii*, which again showed higher values than typical bacterial species.

Primary Sequence Analysis

The primary structure analysis, represented by the amino acid composition chart (Figure 3), highlights the relative abundance of amino acids within the FabI enzyme. Ala, is the most prevalent amino acid, comprising 16% of the total sequence, followed by Leu at 13.1%, Asparagine at 12.7%, Gly at 12.1%, and Ser at 10.6 (Figure 3). In contrast, several amino acids occur at very low frequencies. Tryptophan is the least abundant, accounting for only 1.2%, followed by Cys at 1.9% and His at 2.9%. The low proportion of Cys is particularly notable and suggests a minimal role in disulfide bond formation or catalytic stabilization within the overall protein structure.

A motif analysis of 25 FabI protein sequences (Figure 4) revaeled that Motif 2 (FRKMLAHCEAVTPJRRTVTI-EDVGNSAAFLCSDLSAGISGEVLHVDGGFS) and Motif 3 (FLTGKRILVTGVASKLSIAYGIAQAMHREGAELAF TYQNEK) were present across all 25 sequences. By contrast, Motif 1 (YLGAERAIPNYNVMGLAKASLEANVRYMANAM GPEGVRVNAISAGPIRTL) was found exclusively in bacterial sequences, with complete absence in the five parasitic FabI sequences. Additionally, although motif architecture in bacterial sequences showed highly consistent spatial arrangement and spacing, parasitic sequences demonstrated variability in motif positioning.

Table 1. Physicochemical properties of FabI enzymes.

Organism	Length	Molecular weight	pI	AI	II	GRAVY	EC	R-	R+
Bacillus cereus	256	27740.46	5.45	97.54	34.38	-0.048	13075	33	26
B. subtilis	258	27873.74	5.67	97.21	37.09	0.017	14565	31	25
Cedecea neteri	263	28001.1	5.32	93.95	20.68	0.162	16180	31	24
C. cayetanensis	393	40696.96	6.01	84.07	35.55	-0.083	30495	39	35
E. tenella (Coccidian parasite)	410	42856.81	6.86	91.46	38.31	0.046	27390	38	38
E. faecalis	250	26766.7	5.29	105.72	13.22	0.124	19035	29	24
E. coli	262	27863.94	5.58	92.44	21.14	0,163	16180	29	24
Haemophilus influenzae	262	28119.1	5.35	92.18	23.65	0.07	17545	31	26
H. pylori	275	29981.45	7.1	100.04	27.5	0,012	28880	27	27
Klebsiella oxytoca	262	27909.01	5.59	93.97	27.39	0.151	21680	29	24
Lonsdalea populi	262	27862.81	5.15	94.31	23.56	0.184	14690	29	22
N. caninum	411	43022.49	7.11	81.34	35.78	-0.094	48360	39	39
P. falciparum	432	49755.30	9.11	77.92	45.92	-0.683	45395	47	57
Plesiomonas shigelloides (Aeromonas shigelloides)	263	27805.71	5.39	92.17	28.07	0.169	17670	28	22
P. gergoviae (Enterobacter gergoviae)	262	28014.15	5.77	94.35	21.11	0.145	20190	29	25
Proteus vulgaris	262	28234.34	5.48	89.85	22.04	0.023	19035	31	26
Pseudocitrobacter	262	28015.13	5.6	94.69	24.84	0.148	17670	29	24
P. aeruginosa	265	28005.82	5.64	85.92	24.03	0.028	20065	30	26
Raoultella terrigena (Klebsiella terrigena)	262	27928.05	5.6	94.103	25.08	0.174	16180	29	24
R. conorii	260	28211.34	7.71	91.23	24.55	-0.059	31525	25	26
S. typhimurium	262	27760.82	5.57	92.44	20.58	0.191	16180	28	23
S. praecaptivus	262	27916.86	5.37	92.48	26.1	0.175	17670	27	21
S. aureus	256	27991.87	5.64	99.8	33.91	-0.143	13410	33	28
T. gondii	417	43658.17	8.54	85.25	34.87	-0.086	41370	37	39
Yersinia ruckeri	262	27889.98	5.59	92.48	24.77	0.159	16180	28	23

InterPro analysis of Motif 1, Motif 2, and Motif 3 further confirmed that all three motifs map to a single conserved functional domain, corresponding to the NAD(P) binding Rossmann-fold domain.

Secondary Structure Composition of FabI Enzymes

Analysis of predicted secondary structure composition for FabI enzymes across bacterial and protozoan taxa revealed conserved structural features along with notable taxonomic differences (Table 2). Alpha helices represented the predominant secondary structural element in all FabI enzymes, consistently accounting for more than 42% of the sequences, with *P. falciparum* displaying the highest value at 49.77%.

In contrast, protozoan FabI enzymes exhibited lower proportions of extended strands (9.92%–14.39%) and beta turns (5.12%–6.94%) compared with bacterial sequences, which typically contained extended strands ranging from 15.65% to 19.38%, and beta turns between 7.31% and 9.16%. Correspondingly, FabI proteins from *Cyclospora cayetanensis*, *Eimeria tenella*, *Neospora caninum*, and *T. gondii* contained notably higher proportions of random coils (35.49%–38.42%) than most bacterial FabI enzymes (25%–31%), with *P. falciparum* serving as an exception among protozoa at 30.56%.

Significantly, the prediction for disulfide bridges was "none" across all FabI sequneces analyzed, indicating a consistent absence of disulphide-bond stabilization within the predicted structures.

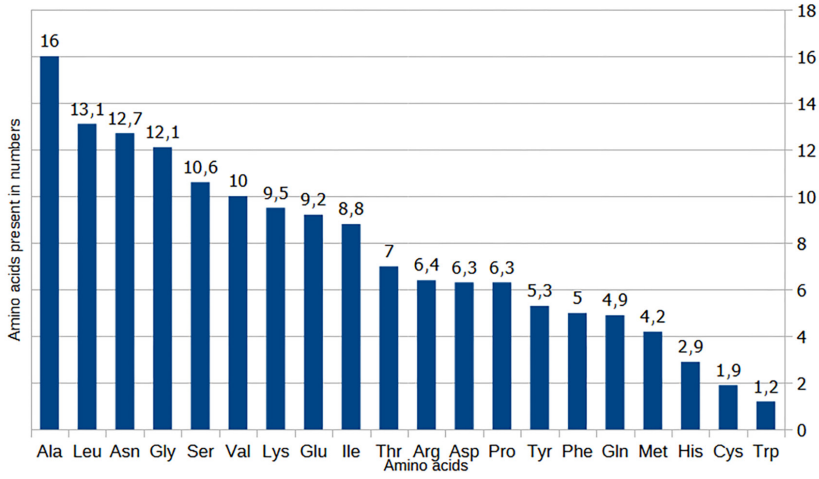

Figure 3. Amino acid composition of FabI enzymes.

Table 2. Predicted secondary structure composition of FabI Enzymes from various organisms.

Organism	Entry	Alpha helix	Extended strand	Beta turn	Random coil	Disulfide bridges prediction
B. cereus	Q81GI3	45.70%	18.36%	7.42%	28.52%	None
B. subtilis	P54616	43.02%	19.38%	8.91%	28.68%	None
C. neteri	A0A291DXE3	44.11%	18.25%	8.37%	29.28%	None
C. cayetanensis	A0A6P6RXR9	45.55%	9.92%	6.11%	38.42%	None
E. tenella (Coccidian parasite)	Q0VIP6	46.83%	12.20%	5.12%	35.85%	None
E. faecalis	Q820V5	46.40%	18.80%	8.00%	26.80%	None
E. coli	P0AEK4	45.80%	17.94%	8.02%	28.24%	None
H. influenzae	P44432	43.89%	17.56%	8.02%	30.53%	None
H. pylori (Campylobacter pylori)	O24990	45.09%	16.73%	8.00%	30.18%	None
K. oxytoca	A0A181Y691	43.13%	18.70%	9.16%	29.01%	None
L. populi	A0A3N0UVW2	45.04%	15.65%	8.40%	30.92%	None
N. caninum	A0A0F7URG4	45.26%	12.17%	5.84%	36.74%	None
P. falciparum	Q965D5	49.77%	12.73%	6.94%	30.56%	None
P. shigelloides (Aeromonas shigelloides)	A0A379CMF8	44.87%	16.35%	8.37%	30.42%	None

Table 2. Continued.

Organism	Entry	Alpha helix	Extended strand	Beta turn	Random coil	Disulfide bridges prediction
Pluralibacter gergoviae (Enterobacter gergoviae)	A0A089PP31	45.80%	17.18%	8.40%	28.63%	None
P. vulgaris	A0A6G6SGP5	47.71%	16.79%	8.40%	27.10%	None
Pseudocitrobacter	A0A5B0K471	47.71%	17.18%	8.40%	26.72%	None
P. aeruginosa	Q9ZFE4	44.53%	16.98%	8.30%	30.19%	None
R. terrigena (Klebsiella terrigena)	A0A485BDY1	46.56%	18.32%	8.40%	26.72%	None
R. conorii	Q92IC6	42.31%	19.23%	7.31%	31.15%	None
Salmonella typhimurium	P16657	44.66%	18.32%	8.02%	29.01%	None
Sodalis praecaptivus	W0HT04	45.04%	16.79%	7.63%	30.53%	None
S. aureus	Q6GI75	42.19%	18.36%	8.98%	30.47%	None
T. gondii	Q6UCJ9	43.88%	14.39%	6.24%	35.49%	None
Y. ruckeri	A0A085U7S9	48.47%	17.18%	8.78%	25.57%	None

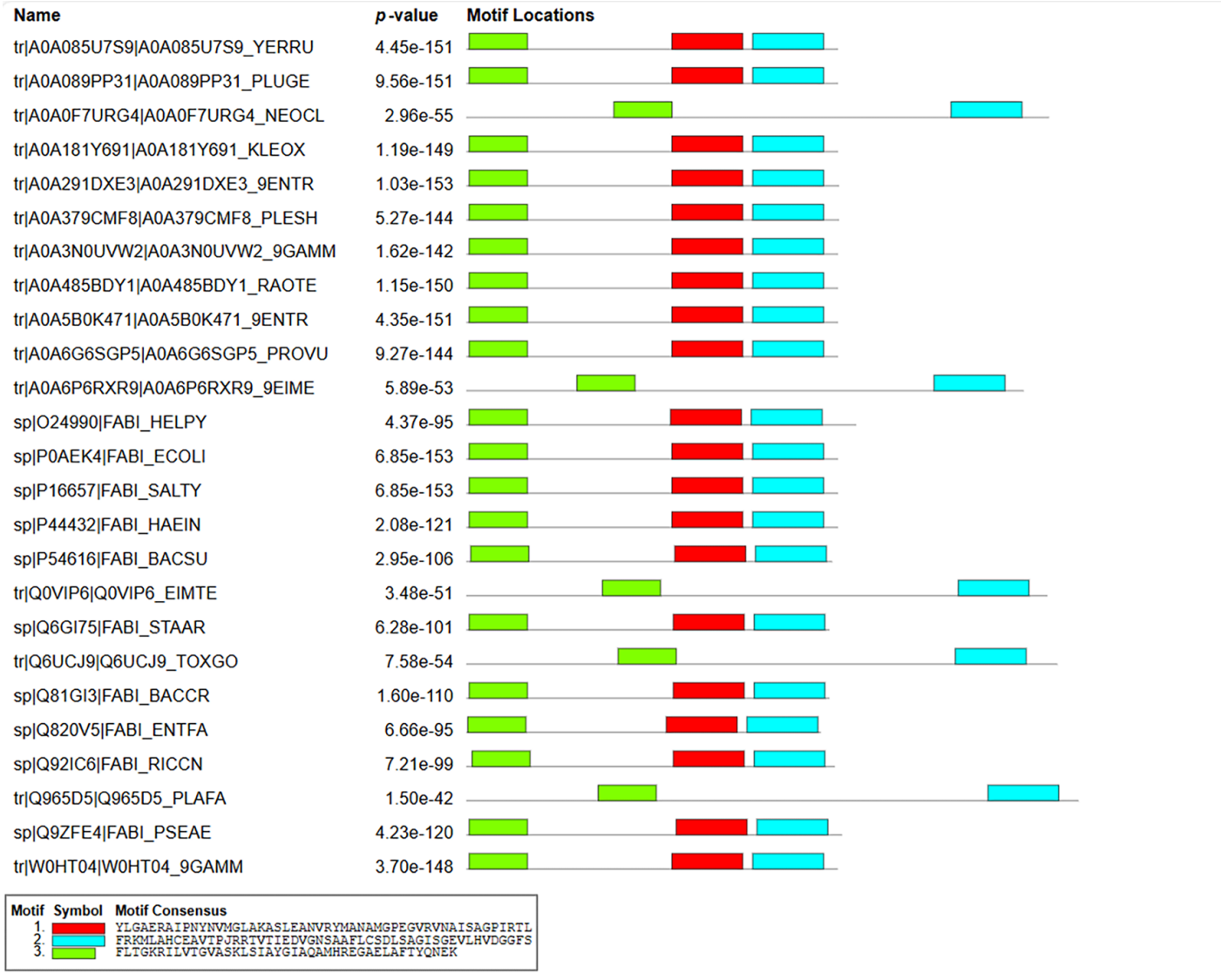

Figure 4. Conserved motifs identified in FabI enzyme sequences.

Further structural interpretation via PDBsum, generated using the predicted *P. falciparum* FabI structure as a reference model (Figure 5), revealed a mixed alpha/beta fold typical of metabolic enzymes.

The FabI structure is predominantly helical, comprising 19 alpha helices (H1–H19) (Figure 6), distributed throughout the polypeptide chain, along with 9 beta-strands forming multiple beta sheets that contribute to the protein's core stability. These regular secondary structure elements are interconnected via loops and turns, forming the characteristic topological arrangement depicted in the PDBsum analysis.

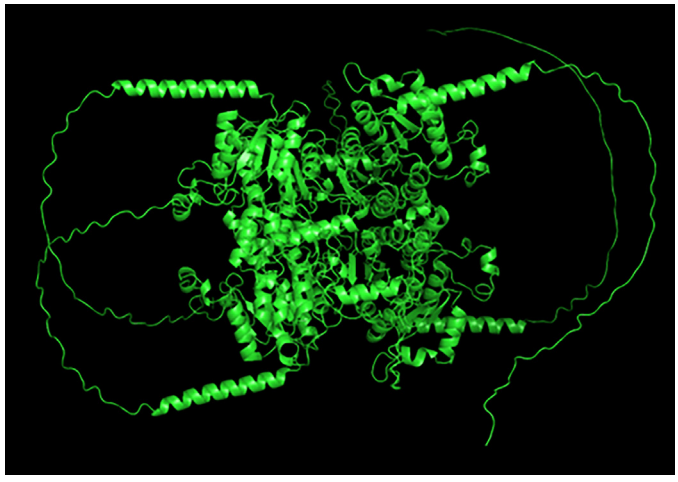

Figure 5. Predicted 3D structure of *P. falciparum* FabI enzyme.

Tertiary Structure Analysis

The stereochemical quality of the predicted FabI enzyme structure was assessed using a Ramachandran plot generated by PROCHECK (Figure 7). The results demonstrated that the majority of amino acid residues occupy energetically favorable conformational regions. Specifically, 71.5% (1144 residues) were located in the most favored regions, while 21.8% (349 residues) fell within additionally allowed regions. A further 6.4% (103 residues) were present in generously allowed regions. Only 4 residues (0.2%) appeared in disallowed regions. Given that 1600 non-Gly and non-Proline (Pro) residues were evaluated (with Gly and Pro excluded due to their atypical conformational flxibility), this extremely low percentage of disallowed residues indicates high stereochemical quality and provides strong confidence in the predicted FabI model.

ERRAT analysis was subsequently performed to evalaute overall and local model quality (Figure 8). The predicted structure achieved an Overall Quality Factor of 78.71%. The ERRAT output highlights several regions with elevated error values, indicated by prominent red peaks. These occur primarily within the residue ranges 20–40 and 120–130, where error values approach the 95% rejection limit.

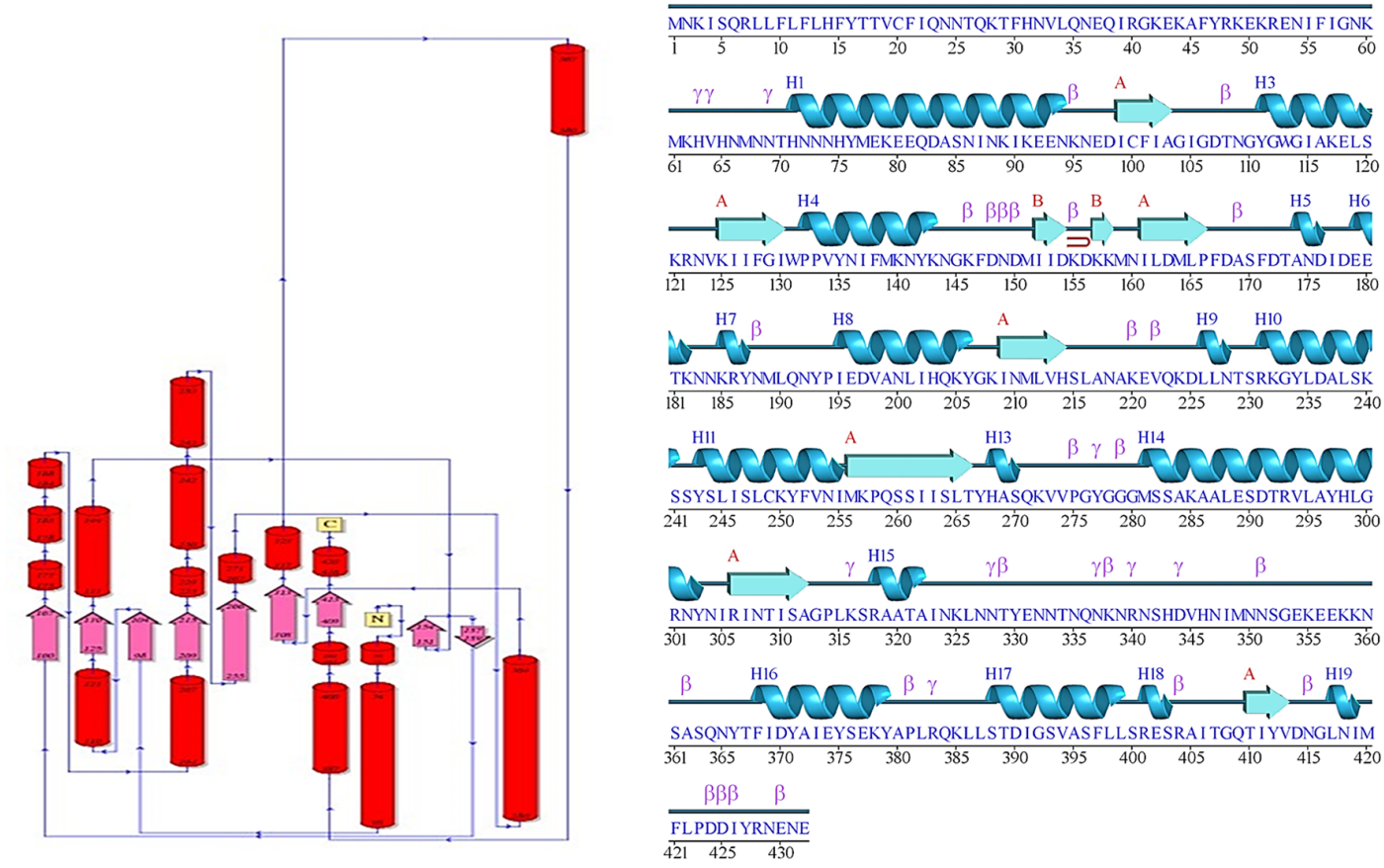

Figure 6. PDBsum analysis showing the predicted structural features of the FabI enzyme.

Local model reliability was further assessed through the Local Quality Estimate plot (Figure 9), which provides confidence values on a per-residue basis. For most of the structure (approximately residue 75 onward), the predicted confidence remains consistently above 0.7, indicating high accuracy in these regions.

In contrast, the N-terminal segment (residues 0–75) displays substnatially lower confidence, with scores frequently dropping below 0.5 and, in several positions, approaching 0.1. Additionally but comparatively minor dips in confidence occur near residue 330 and toward the C-terminus region beyond residue 380.

Functional Analysis

Signal Peptide Prediction

The N-terminal sequence of the FabI enzyme was examined using SignalP 6.0 to determine the presence and likely location of a signal peptide (Figure 10). The prediction profile displays a prominent n-region (Sec/SPI n, solid red line) at the extreme N-terminus, corresponding to a positively charged stretch. This is followed by a strong hydrophobic h-region (Sec/SPI h, orange line), which extends from approximately residue 3 to residue 15, and peaks near residue 10.

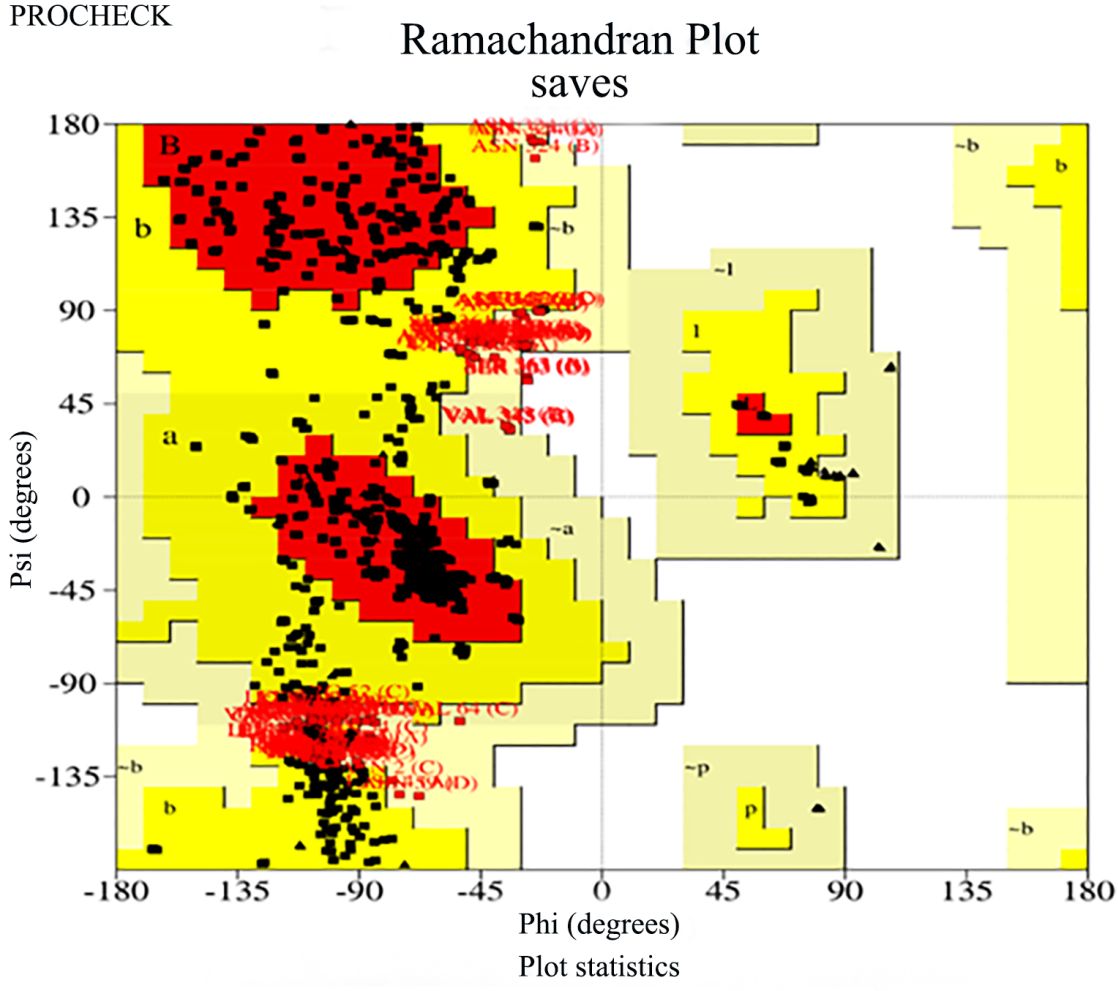

Figure 7. Ramachandran plot for the predicted *P. falciparum* FabI structure, generated by PROCHECK.

Subsequently, the c-region (Sec/SPI c, yellow line) reaches its maximum probability around residue 24, indicating the most likely cleavage site. After residue 25, the probability for "OTHER" (non-signal peptide regions, dashed red line) increases sharply, marking the transition into the mature protein. Collectively, these predicted profiles indicate a canonical Sec/SPI signal peptide at the N-terminal region, with the cleavage site estimated between residues 22 and 25.

In Silico Proteolytic Digestion

An *in silico* proteolytic digestion analysis was carried out to predict potential cleavage sites and fragment numbers across the FabI enzyme using multiple proteases and chemical reagents (Table 3). The number of predicted cleavage events varied widely, ranging from a single cut to as many as 194, depending on protease specificity.

Proteinase K showed the highest cleavage frequency, with 194 predicted sites, followed by Thermolysin (120 cleavage sites), Pepsin at pH > 2 (98 cleavage sites), and Chymotrypsin (low-specificity) (94 cleavage sites), all of which would generate numerous small peptide fragments.

In contrast, enzymes with narrow specificity, such as Caspase1 and Pro endopeptidase, produced only a single predicted cleavage event. Similarly, BNPS-Skatole and Iodosobenzoic acid each generated two cuts, while Hydroxylamine and NTCB produced three cuts. Enzymes with moderate specificity, such as Trypsin (54 cleavages) and high specificity-Chymotrypsin (40 cleavages), yielded intermediate fragmentation patterns.

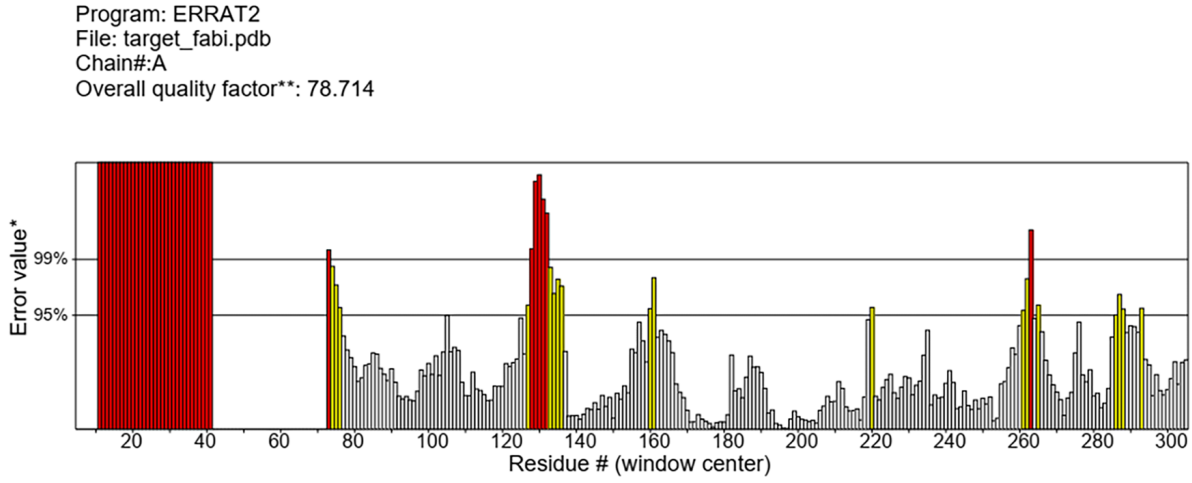

Figure 8. ERRAT plot for the predicted *P. falciparum* FabI enzyme structure.

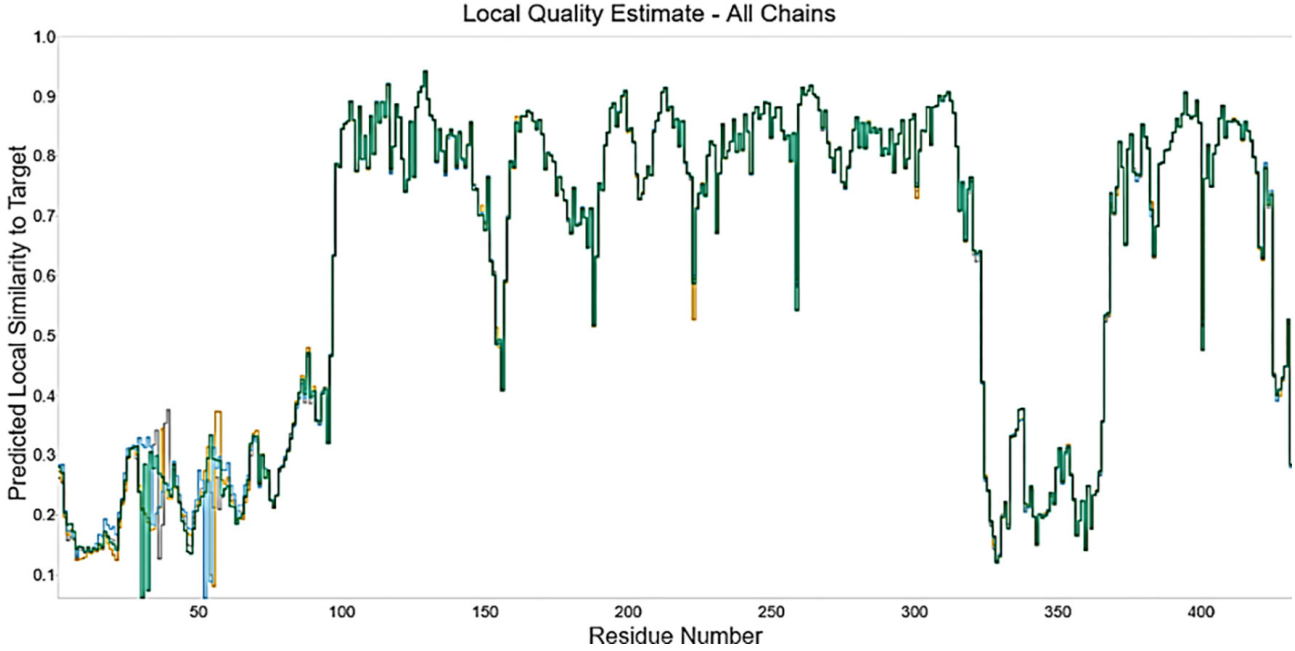

Figure 9. Local quality estimate of the predicted *P. falciparum* FabI structure, showing per-residue confidence scores.

Characterization of Active Site and Other Pockets via CASTp 3.0

The CASTp 3.0 server was used to perform a detailed topological analysis of the *P. falciparum* FabI protein, with particular emphasis on the characterization of active site pockets. The most prominent active site was represented by four discrete pocket instances, exhibiting solvent-accessible surface areas of 8.368 Å², 8.360 Å², 8.375 Å², and 8.147 Å², with corresponding volumes of 43.996 Å³, 43.763 Å³, 43.429 Å³, and 43.133 Å³, respectively. Functionally important residues identified within these pockets included Tyr267, His268, Ser311, Ala312, Gly313, and Pro314, Ala372, Tyr375, and Asp414.

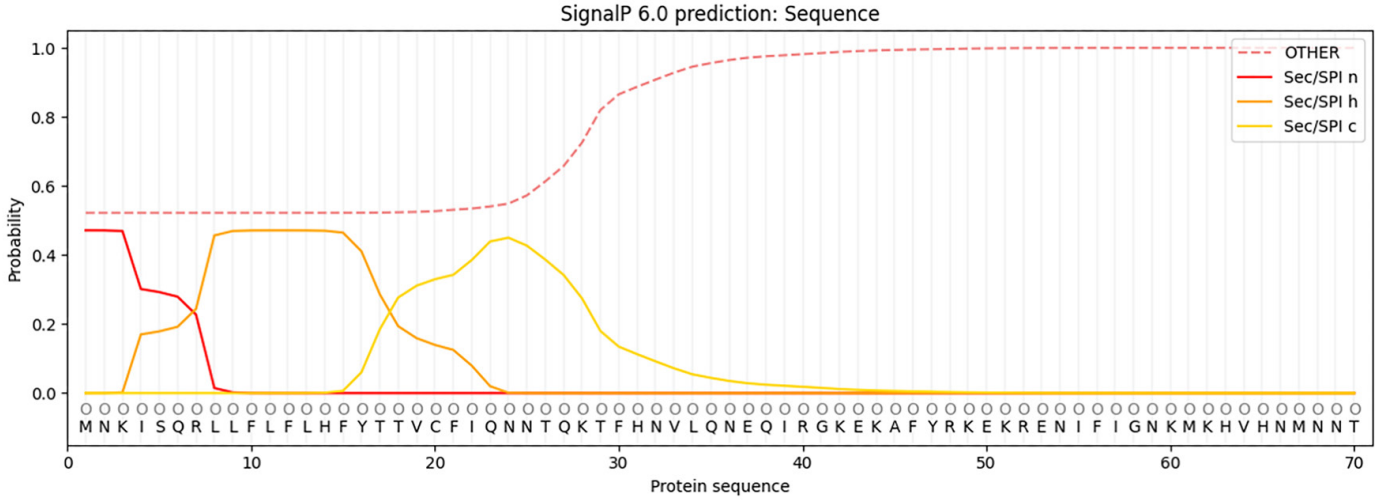

Figure 10. SignalP 6.0 prediction of the *P. falciparum* FabI N-terminal sequence, illustrating probabilities for n-region (Sec/SPI n), h-region (Sec/SPI h), c-region (Sec/SPI c), and non-signal peptide (OTHER).

Table 3. Predicted proteolytic cleavage sites for *P. falciparum* FabI enzyme.

Name of enzyme	Number of cleavages	Positions of cleavage sites
Arg-C proteinase	16	7 40 48 52 122 186 231 293 301 306 318 340 383 401 404 428
Asp-N endopeptidase	22	82 97 106 147 149 153 155 162 167 171 175 177 196 224 235 290 343 369 389 413 423 424
Asp-N endopeptidase + N-terminal Glu	47	36 42 49 52 77 79 80 82 91 92 96 97 106 117 147 149 153 155 162 167 171 175 177 178 179 195 196 220 224 235 288 290 330 343 353 355 356 369 373 376 389 401 413 423 424 429 431
BNPS-Skatole	2	113 131
Caspase1	1	390
Chymotrypsin-high specificity (C-term to [FYW], not before P)	40	10 12 15 16 21 30 46 47 56 76 101 111 113 128 135 138 142 147 167 171 187 206 234 243 251 252 267 277 297 303 330 366 368 371 375 379 397 412 421 427
Chymotrypsin-low specificity (C-term to [FYWML], not before P)	94	1 8 9 10 11 12 13 14 15 16 21 30 31 34 46 47 56 61 63 65 67 71 75 76 77 101 111 113 119 128 135 138 139 142 147 151 159 162 164 167 171 187 189 190 201 203 206 211 212 214 216 226 227 234 235 238 243 245 248 251 252 256 265 267 268 277 281 288 295 297 298 299 303 315 326 330 346 349 366 368 371 375 379 382 386 387 397 398 399 412 417 420 421 427
Clostripain	16	7 40 48 52 122 186 231 293 301 306 318 340 383 401 404 428
CNBr	14	1 61 67 77 139 151 159 164 189 211 256 281 349 420
Formic acid	22	83 98 107 148 150 154 156 163 168 172 176 178 197 225 236 291 344 370 390 414 424 425
Glutamyl endopeptidase	25	37 43 50 53 78 80 81 92 93 97 118 179 180 196 221 289 331 354 356 357 374 377 402 430 432

Table 3. Continued.

Name of enzyme	Number of cleavages	Positions of cleavage sites
Hydroxylamine	3	109 144 415
Iodosobenzoic acid	2	113 131
LysC	41	3 28 42 44 49 51 60 62 79 89 91 95 117 121 125 140 143 146 155 157 158 182 185 205 208 220 224 232 240 250 257 272 285 316 325 338 355 358 359 378 385
LysN	41	2 27 41 43 48 50 59 61 78 88 90 94 116 120 124 139 142 145 154 156 157 181 184 204 207 219 223 231 239 249 256 271 284 315 324 337 354 357 358 377 384
NTCB (2-nitro-5-thiocyanobenzoic acid)	3	19 99 248
Pepsin (pH > 2)	98	8 10 11 12 13 14 15 20 21 29 34 45 47 55 56 75 76 100 101 110 111 112 113 118 128 135 137 138 141 146 147 161 162 165 166 170 171 189 190 193 200 201 206 211 212 215 225 227 235 237 238 243 244 245 247 248 250 251 264 265 266 267 277 288 294 296 297 298 299 302 314 325 326 329 330 365 366 367 368 370 371 374 375 378 381 386 396 397 398 399 411 412 416 417 420 422 426 427
Pepsin (pH1.3)	66	8 10 11 12 13 14 15 20 21 29 34 45 55 56 100 101 118 128 137 138 146 147 161 162 165 166 170 171 189 190 200 201 211 212 215 225 227 235 237 238 244 245 247 248 251 264 265 288 294 298 299 314 325 326 367 368 381 386 396 397 398 399 416 417 420 422
Pro endopeptidase [*]	1	258
Proteinase K	194	4 8 9 10 11 12 13 15 16 17 18 19 21 22 26 29 30 33 34 37 39 43 45 46 47 50 53 55 56 57 64 70 76 78 80 81 84 87 90 92 93 97 99 101 102 103 105 108 111 113 115 116 118 119 124 126 127 128 130 131 134 135 137 138 142 147 152 153 161 162 165 167 169 171 173 174 177 179 180 181 187 190 193 195 196 198 199 201 202 206 209 212 213 216 217 219 221 222 226 227 229 234 235 237 238 243 245 246 248 251 252 253 255 262 263 265 266 267 269 273 274 277 284 286 287 288 289 292 294 295 296 297 299 303 305 307 309 310 312 315 319 320 321 322 323 326 329 330 331 334 345 348 354 356 357 362 366 367 368 369 371 372 373 374 375 377 379 380 382 386 387 389 391 394 395 397 398 399 402 405 406 407 410 411 412 413 417 419 421 422 426 427 430 432
Staphylococcal peptidase I	21	37 43 50 53 78 80 92 97 118 179 196 221 289 331 354 356 374 377 402 430 432
Thermolysin	120	3 7 8 9 10 11 12 14 18 20 21 29 32 33 38 44 45 54 55 56 60 63 66 76 86 89 100 101 102 104 114 115 123 125 126 127 129 133 136 137 138 146 151 152 158 160 161 166 170 173 188 189 194 198 200 201 208 210 211 212 215 216 218 226 234 237 244 245 247 251 252 254 255 261 262 264 268 272 280 283 285 286 287 293 294 295 298 304 306 309 311 314 318 319 321 322 325 347 348 361 367 368 371 372 381 385 386 393 394 396 397 398 404 405 410 412 416 418 419 420
Trypsin	54	3 7 28 40 42 44 48 49 51 52 60 62 79 89 91 95 117 121 122 125 140 143 146 157 158 182 185 186 205 208 220 224 231 232 240 272 285 293 301 306 316 318 325 338 340 355 358 359 378 383 385 401 404 428
Total	943	

In addition to these active site pockets, CASTp analysis revealed another large and centerally located pocket with a subtantially greater surface area (951.472 Å²) and volume (851.864 Å³). Key residues lining this central cavity included His268, Ser270, and Glutamine 271 (Gln271), together with Threonine 292 (Thr292), Arginine 293 (Arg293), Tyr412, and Isoleucine 419 (Ile419). The 3D representation of these identified pockets is shown in (Figure 11), where the four active site-associated pockets are highlighted in pink and the centrally loacted pocket is depicted in black.

Discussion

Two highly conserved regions, AKAALES and RVNAISAGPIRT, were identified within FabI enzyme sequences, underscoring their likely functional importance. Although conservation is broadly maintained, several amino acid positions exhibit specific substitutions. Some substitutions retain similar physicochemical properties (conservative), while others introduce marked changes (non-conservative).

In the AKAALES region, Ala329 occasionally undergoes a non-conservative substitution to Ser, thereby introducing a polar hydroxyl group in place of the nonpolar methyl group typically resides there. Conversely, Glutamic Acid 331 shows a highly conservative change to Asp since both are acidic, negatively charged amino acids, which ensures that the electrostatic role of the site is preserved. At the position 332, a notable degree of variation is observed, directly influencing the local polarity. The substitution from Ser to Ala is non-conservative because it shifts the residue's characteristic from polar to nonpolar. Furthermore, in one instance, Thr (T) is present at this site. When considering this change, a substitution from Ser to Thr is conservative, as both are polar amino acids possessing similar hydroxyl groups; however, if Ala were replaced by Thr, it would constitute a non-conservative change.

Within the longer RVNAISAGPIRT region, variations at position 349 (Valine to Ile), and at position 352 (Ile to Valine or Leu) are conservative, since all involved amino acids are nonpolar, branched-chain hydrophobics and collectively maintain the local hydrophobic environment. Similarly, the alternations at positions 357 (Leu/Ile), 358 (Lysine/Arg), 359 (Ser/Thr), are also conservative. However, at position 351 (typically Ala) in RVNAISAGPIRT there are diverse non-conservative substitutions to Gly, Ser, Thr, or Cys. These changes can either alter local flexibility (Gly) or significantly modify the polarity (Ser, Thr, Cys). The Cys substitution is particularly notable because its reactive thiol group could introduce new chemical functionalities. Lastly, the change from Pro to Ala at position 356 is non-conservative, as this substitution, observed in only one instance, fundamentally alters the local structural rigidity. Altogether, these patterns highlight a strategic balance, in which conservative substitutions maintain core function through preservation of essential physicochemical properties, while non-conservative changes may reflect specific evolutionary adaptations that influence enzyme characteristics and could impact activity, substrate specificity, or stability in different host environments.

The phylogenetic analysis of FabI enzyme sequences yields crucial insights into their evolutionary origins and relationships across diverse taxa. A key finding is the clear and substantial evolutionary distance observed between the *Plasmodium*-containing Apicomplexa clade and all bacterial lineages represented in the tree. This distinct separation, in which *Plasmodium*'s FabI clusters tightly with other apicomplexan orthologs yet remains phylogenetically distant from all bacterial FabI sequences, is highly significant because FabI is fundamentally a prokaryotic (bacterial) FAS enzyme. The presence of such a typically bacterial enzyme

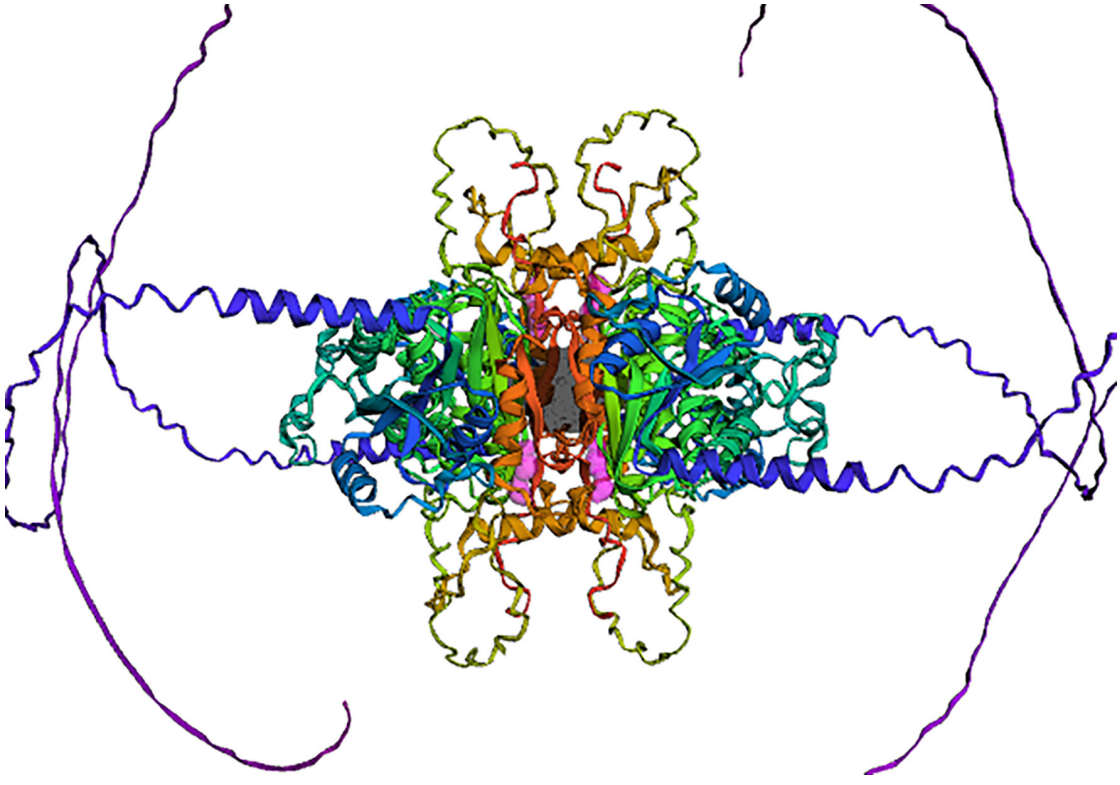

Figure 11. 3D representation of *P. falciparum* FabI enzyme, highlighting predicted CASTp 3.0 pockets. The four active site-related pockets are shown in pink, and another significant central pocket is depicted in black.

within a eukaryotic parasite like *Plasmodium*, as evidenced by its unique branching pattern in the tree, strongly supports its acquisition through an ancient horizontal gene transfer (HGT) event. This transferred gene likely originated from a bacterial ancestor that became endosymbiotic and ultimately gave rise to the apicoplast-a non-photosynthetic plastid within Apicomplexa that houses the bacterial-derived FAS-II pathway. This profound evolutionary divergence of apicomplexan FabI from extant bacterial enzymes together with its distinctness from human FAS pathways, positions it as a highly promising target for anti-parasitic drug development.

The observed distinct physicochemical profiles between protozoan and bacterial FabI enzymes offer valuable insights into their functional adaptations and evolutionary trajectories. The larger size and higher molecular weight of FabI from protozoan parasites, together with their generally higher isoelectric points (pI) and greater hydrophilicity (negative GRAVY values), stand in sharp contrast to the smaller, more hydrophobic, and typically lower pI bacterial FabI. This comparison suggests that protozoan FabI enzymes, such as those in *Plasmodium* with its notably high pI and hydrophilicity, may be specifically adapted for different intracellular environments or protein interaction partners than their bacterial counterparts. For instance, increased hydrophilicity could indicate greater surface exposure or more extensive interactions with the aqueous lumen of the apicoplast, where these enzymes function.

Furthermore, the higher count of charged residues (acidic and basic) in protozoan FabI contributes to their distinct pI values and to potentially more complex electrostatic interactions. While most bacterial FabI display consistent characteristics, the exceptions, such as the higher pI observed in *H. pylori* and *R. conorii*, might reflect adaptations to unique intracellular or extracellular niches and corroborate the distinct branching patterns observed in the phylogenetic analysis.

A motif analysis was performed on 25 FabI protein sequences. Notably, despite the overall conservation of Motif 2 and Motif 3, several parasitic FabI sequences showed shifts in the relative positions of these motifs compared to their bacterial counterparts. Such positional shifts may reflect structural adaptations or domain rearrangements specific to the parasite's cellular environment or evolutionary history. The absence of Motif 1 in protozoan FabI sequences, despite its broad and consistent presence in bacteria, further suggests a significant evolutionary divergence. This indicates that protozoan FabI either performs its function using a different molecular mechanism that does not require Motif 2, or that this region was lost or became highly divergent following the initial HGT event from a bacterial ancestor.

The precise mapping of all three identified conserved motifs to a specific domain within *P. falciparum* FabI provides critical insights into its functional architecture, and this domain's identification as a NAD(P) binding Rossmann-fold domain is highly significant.

The Rossmann fold is a well-established supersecondary structural motif that is essential for binding nucleotides, particularly NAD(P)H, which serves as a vital cofactor for a vast array of oxidoreductases. Given that FabI (enoyl-ACP reductase) is an oxidoreductase that absolutely requires NAD(P)H for its catalytic activity, locating these three conserved motifs precisely within this NAD(P) binding Rossmann-fold domain directly confirms the structural basis for cofactor recognition and enzymatic function. Their presence within this specialized domain also strongly suggests direct involvement in substrate binding, catalysis, or cofactor interaction.

The predicted secondary structure profiles additionally highlight lineage-specific adaptations of FabI enzymes. The predominance of alpha-helical content across all analyzed FabI sequences points to a shared compact globular architecture that is essential for enzymatic function. However, compared to their bacterial counterparts, protozoan FabI enzymes generally contain lower proportions of extended strands and beta turns while exhibiting higher random coil content, indicating a potentially greater inherent flexibility. Notably, *P. falciparum* is distinct among protozoa, with a random coil percentage more closely aligned with bacterial FabI, suggesting a particular structural adaptation possibly tied to unique functional requirements or its intracellular environment. Most significantly, the universal absence of predicted disulfide bridges across all FabI enzymes strongly indicates that these proteins operate in reducing cellular environments, such as the bacterial cytoplasm or the apicoplast lumen, where stabilizing bonds are not typically formed.

The ERRAT analysis provided a important assessment of the predicted FabI enzyme structure. Although the overall quality factor suggests a plausible structural model, the most prominent areas of concern are highly localized within the N-terminal region, particularly around residues 20–40. This clustering of high error values (red spikes) is strongly suggestive of a cleavable N-terminal signal or transit peptide. Because *P. falciparum* FabI is known to be targeted to the apicoplast, such targeting sequences are inherently flexible or unstructured in the mature protein and are normally cleaved off following import into the organelle. As a result, computational modeling tools frequently struggle to accurately predict the conformation of these dynamic or absent regions, leading to their erroneous classification by quality assessment programs like ERRAT. For this reason, the localized discrepancy does not invalidate the accuracy of the predicted 3D structure of the mature, functional FabI enzyme.

The Local Quality Estimate plot provides a crucial residue-level assessment of the predicted FabI enzyme structure and offers insights into the reliability of different regions. Across the majority of the protein, the confidence scores remain generally high (typically above 0.7 from residue ~75 onwards), which is encouraging and suggest that the previously described core structural elements and overall fold are well-predicted and represent a reliable model for the mature, functional enzyme.

In contrast, the N-terminal segment (residues 0 to ~75) displays a prominent and consistent region of significantly low confidence, and this pattern constitues a key observationthat warrants specific discussion. The same region has been highlighted in the ERRAT

plot through high error values, and the agreement between between both analyses strongly supports the interpretation that this segment reprsents an intrinsically disordered or highly flexible N-terminal signal/transit peptide.

This conclusion is further supported by SignalP 6.0, which predicts a cleavable signal peptide with a likley cleavage site near residues 22–25, consistent withprevious indicators that the N-terminus remains unstructured before processing.

The *in silico* proteolytic digestion analysis also provides a useful guidance for future biochemical characterization of *P. falciparum* FabI. The wide range in predicted cleavage events, from a single cut to almost 200, reflects the diverse specificities of the proteases and chemical reagents tested.

Broad specificity enzymes such as Proteinase K, Thermolysin, Pepsin, and low-specificity Chymotrypsin are effective for extensive digestion, which may be useful for amino acid composition analysis or generating small peptides for mass spectrometry identification.

Conversely, proteases like Caspase1 and Pro-endopeptidase, which each yield only one cleavage site, are highly selective and therefore valuable for isolating large, well-defined fragments for structural studies or targeted protein engineering. Limited cleavage by chemical reagents such as BNPS-Skatole and Hydroxylamine similarly confirms their utility for generating a few large peptides by acting on less common amino acid residues. Together, this cleavage map forma an important foundation for experimental design, including peptide fingerprinting, structural domain isolation, and verifying recombinant protein integrity.

The CASTp 3.0 analysis further contributes by characterizing the surface features and internal topography of the FabI enzyme.

The prominent active site appears as four relatively small pocket instances (each with areas of 8 Å² and volumes of 43 Å³), suggesting a more complex architecture than a single cavity. These multiple sub-pockets may accommodate different substrate regions or catalytic intermediates involved in multi-step FAS. The central cavity could also function as an allosteric binding site, a channel for substrate/product passage, or a location involved in conformational shifts. Altogether, these detailed topographical insights are invaluable for understanding catalytic mechanism, predicting ligand binding, and guiding inhibitor design.

Conclusion

This comprehensive computational structural and functional study has meticulously characterized the *P. falciparum* FabI enzyme, which serves as a critical antimalarial target. The work provides a robust foundation for researchers to gain a detailed understanding of its protein structure, thereby facilitating the rational design of novel compounds with desirable characteristics for exploiting them as potential drug targets against malaria. However, further experimental (*in vitro* and *in vivo*) studies are essential to validate these computational predictions.

Ethics

Ethics Committee Approval: Not required.

Data Sharing Statement: All data are available within the study.

Footnotes

Authorship Contributions: Concept: D.J.; Design: D.J.; Execution: A.B., H.A., D.J.; Data acquisition: A.B., H.A.; Data analysis/interpretation: D.J.; Writing: A.B., H.A., D.J.; Critical review: D.J.

Conflict of Interest: The authors have no conflicts of interest to declare.

Funding: The authors declared that this study has received no financial support.

References

Bailey, T. L., & Elkan, C. (1994). Fitting a mixture model by expectation maximization to discover motifs in biopolymers. *Proceedings of the International Conference on Intelligent Systems for Molecular Biology, 2*, 28–36. https://pubmed.ncbi.nlm.nih.gov/7584402/

Benkert, P., Biasini, M., & Schwede, T. (2010). Toward the estimation of the absolute quality of individual protein structure models. *Bioinformatics, 27*(3), 343–350. https://doi.org/10.1093/bioinformatics/btq662

Blum, M., Andreeva, A., Florentino, L. C., Chuguransky, S. R., Grego, T., Hobbs, E., Pinto, B. L., Orr, A., Paysan-Lafosse, T., Ponamareva, I., Salazar, G. A., Bordin, N., Bork, P., Bridge, A., Colwell, L., Gough, J., Haft, D. H., Letunic, I., Llinares-López, F., ... Bateman, A. (2024). InterPro: The protein sequence classification resource in 2025. *Nucleic Acids Research, 53*(D1), D444–D456. https://doi.org/10.1093/nar/gkae1082

Colovos, C., & Yeates, T. O. (1993). Verification of protein structures: Patterns of nonbonded atomic interactions. *Protein Science, 2*(9), 1511–1519. https://doi.org/10.1002/pro.5560020916

Gasteiger, E., Hoogland, C., Gattiker, A., Wilkins, M. R., Appel, R. D., & Bairoch, A. (2005). Protein identification and analysis tools on the ExPASy server. In *Humana Press eBooks* (pp. 571–607). https://doi.org/10.1385/1-59259-584-7:531

Geourjon, C., & Deléage, G. (1995). SOPMA: Significant improvements in protein secondary structure prediction by consensus prediction from multiple alignments. *Bioinformatics, 11*(6), 681–684. https://doi.org/10.1093/bioinformatics/11.6.681

Hopf, F. S. M., Roth, C. D., De Souza, E. V., Oliveira, S. A., & Zamboni, D. S. (2022). Bacterial enoyl-reductases: The ever-growing list of Fabs, their mechanisms, and inhibition. *Frontiers in Microbiology, 13,* 891610. https://doi.org/10.3389/fmicb.2022.891610

Kane, N. F., Kyama, M. C., Nganga, J. K., Hassanali, A., Diallo, M., & Kimani, F. T. (2022). Expression of the Fab enzymes (FabI and FabZ) from *Plasmodium falciparum* after exposure to *Artemisia afra* plant extracts and drugs screening. *Journal of Parasitic Diseases, 47*(1), 46–58. https://doi.org/10.1007/s12639-022-01537-8

Laskowski, R. A., Rullmann, J. A. C., MacArthur, M. W., Kaptein, R., & Thornton, J. M. (1996). AQUA and PROCHECK-NMR: Programs for checking the quality of protein structures solved by NMR. *Journal of Biomolecular NMR, 8*(4), 477–486. https://doi.org/10.1007/bf00228148

Madeira, F., Madhusoodanan, N., Lee, J., Squires, G., Lopez, R., & Künsting, M. (2024). The EMBL-EBI Job Dispatcher sequence analysis tools framework in 2024. *Nucleic Acids Research, 52*(W1), W521–W525. https://doi.org/10.1093/nar/gkae241

Mirdita, M., Schütze, K., Moriwaki, Y., Heo, L., Ovchinnikov, S., & Steinegger, M. (2021). ColabFold: Making protein folding accessible to all. *bioRxiv*. https://doi.org/10.1101/2021.08.15.456425

Pandey, A., Shyamal, S. S., Shrivastava, R., Ekka, S., & Mali, S. N. (2022). Inhibition of *Plasmodium falciparum* fatty acid biosynthesis (FAS-II pathway) by natural flavonoids: A computer-aided drug designing approach. *Chemistry Africa, 5*(5), 1469–1491. https://doi.org/10.1007/s42250-022-00449-7

Pandey, A. K., Siddiqui, M. H., & Dutta, R. (2019). Drug-likeness prediction of designed analogues of isoniazid standard targeting FabI enzyme regulation from *P. falciparum*. *Bioinformation, 15*(5), 364–368. https://doi.org/10.6026/97320630015364

Studer, G., Biasini, M., & Schwede, T. (2014). Assessing the local structural quality of transmembrane protein models using statistical potentials (QMEANBrane). *Bioinformatics, 30*(17), i505–i511. https://doi.org/10.1093/bioinformatics/btu457

Studer, G., Rempfer, C., Waterhouse, A. M., Gumienny, R., Haas, J., & Schwede, T. (2019). QMEANDisCo—Distance constraints applied on model quality estimation. *Bioinformatics, 36*(6), 1765–1771. https://doi.org/10.1093/bioinformatics/btz828

Teufel, F., Armenteros, J. J. A., Johansen, A. R., Gíslason, M. H., Pihl, S. I., Tsirigos, K. D., Winther, O., Brunak, S., von Heijne, G., & Nielsen, H. (2022). SignalP 6.0 predicts all five types of signal peptides using protein language models. *Nature Biotechnology, 40*(7), 1023–1025. https://doi.org/10.1038/s41587-021-01156-3

The UniProt Consortium. (2024). UniProt: The universal protein knowledgebase in 2025. *Nucleic Acids Research, 53*(D1), D609–D617. https://doi.org/10.1093/nar/gkae1010

Tian, W., Chen, C., Lei, X., Zhao, J., & Liang, J. (2018). CASTp 3.0: Computed atlas of surface topography of proteins. *Nucleic Acids Research, 46*(W1), W363–W367. https://doi.org/10.1093/nar/gky473

Supplementary Table 1. https://d2v96fxpocvxx.cloudfront.net/cf9d60d6-523c-458a-a2e6-78728d3ffbb0/content-images/79ec0824-5970-44ed-8b1b-ef7d7f763f5e.pdf